Journal of Theoretical Biology 481 (2019) 61–74

Contents lists available at ScienceDirect

Journal of Theoretical Biology

journal homepage: www.elsevier.com/locate/jtb

A free boundary model of epithelial dynamics

Ruth E Baker[a,*], Andrew Parker[a], Matthew J Simpson[b]

[a] Mathematical Institute, University of Oxford, Oxford, UK
[b] School of Mathematical Sciences, Queensland University of Technology, Brisbane, Australia

ARTICLE INFO

Article history:
Received 16 September 2018
Revised 11 December 2018
Accepted 18 December 2018
Available online 19 December 2018

Keywords:
Cell-based model
Individual-based model
Mechanical model
Cell migration
Cell proliferation
Free boundary problem
Moving boundary problem

ABSTRACT

In this work we analyse a one-dimensional, cell-based model of an epithelial sheet. In the model, cells interact with their nearest neighbouring cells and move deterministically. Cells also proliferate stochastically, with the rate of proliferation specified as a function of the cell length. This mechanical model of cell dynamics gives rise to a free boundary problem. We construct a corresponding continuum-limit description where the variables in the continuum limit description are expanded in powers of the small parameter $1/N$, where N is the number of cells in the population. By carefully constructing the continuum limit description we obtain a free boundary partial differential equation description governing the density of the cells within the evolving domain, as well as a free boundary condition that governs the evolution of the domain. We show that care must be taken to arrive at a free boundary condition that conserves mass. By comparing averaged realisations of the cell-based model with the numerical solution of the free boundary partial differential equation, we show that the new mass-conserving boundary condition enables the coarse-grained partial differential equation model to provide very accurate predictions of the behaviour of the cell-based model, including both evolution of the cell density, and the position of the free boundary, across a range of interaction potentials and proliferation functions in the cell based model.

1. Introduction

Cell biology experiments typically produce complex, quantitative experimental data that can include both cellular-level and tissue-level information (Jin et al., 2016; Maini et al., 2004a; 2004b; Treloar et al., 2014). However, it can often difficult to integrate these multi-scale data to give new insights. This challenge provides a clear motivation for the use of mathematical models where individual, cell-based mechanisms can be implemented and explored in a computational framework (Anderson and Chaplain, 1998; Osborne et al., 2017; Simpson et al., 2013; Turner et al., 2004). This approach can allow us to qualitatively explore the relationship between individual-level properties and population-level outcomes using repeated computational simulations as well as comparing predictions of different models that act at different scales (Murray et al., 2011; Pathmanathan et al., 2009). Furthermore, it is possible to provide a quantitative, more rigorous mathematical connection between the individual-level properties and population-level outcomes by using coarse-graining techniques to derive an approximate continuum-limit description of the individual-level description (Murray et al., 2009; 2012; O'Dea and King, 2012).

Depending on the biological context, there are many different kinds of individual-based models that can be used to simulate cell biology processes including random walk frameworks involving point particles (Browning et al., 2018; Cai et al., 2007) or random walk frameworks based on an exclusion process that explicitly account for excluded volume effects as well as the shape and size of the individuals in the system (Jin et al., 2018; Parker et al., 2018). While discrete models based on point particles and exclusion processes have been successfully applied to study many cell biology phenomena, these models do not include any mechanical effects that are known to be important in a host of applications. For example, tissue stiffness is known to play a key role in epithelial cancer progression, with different rates of invasion associated with different tissue stiffness conditions (Samuel et al., 2011). Cancer detection is another clinical application where tissue mechanics and tissue stiffness, in terms of mammographic density, is thought to be associated with breast cancer risk (Huo et al., 2014). Therefore, for certain applications, it is relevant to use a mechanical framework to study the motion and interaction of individual cells rather than focusing on a random walk framework.

* Corresponding author.
E-mail address: ruth.baker@maths.ox.ac.uk (R.E. Baker).

https://doi.org/10.1016/j.jtbi.2018.12.025

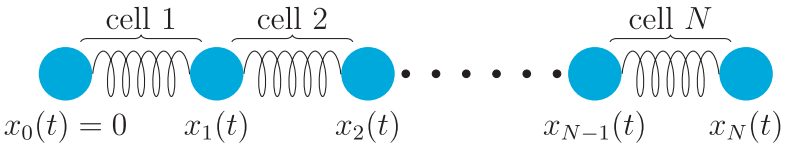

Fig. 1. Schematic of the cell-based model where the cells are here represented by springs and nodes the points where two cells touch. There are N cells, and node positions are denoted by x_i, for $i = 0, 1, \ldots, N$, with the left boundary of the first cell (*i.e.* node 0) fixed at the origin so that $x_0(t) \equiv 0$.

In this work we re-examine a mechanical model of epithelial tissue mechanics first presented by Murray et al. (2009, 2012). The model describes, for example, the one-dimensional cross-section of apical surfaces of a population of N epithelial cells, where nearest neighbour cells interact through a force potential and the motion of each individual is governed by an overdamped, deterministic equation of motion. Like Murray et al. (2009, 2012), we consider the case where the left-most boundary of the population of cells is fixed at $x = 0$, and the right-most boundary is a free boundary, $x = L(\tau)$, where τ is time. In the first part of our work we consider a non-proliferative population where individual cells undergo movement only. In this context the cell-based model is deterministic and the evolution of the free boundary is the net result of the deterministic interactions between the N individuals. In the second part of our work we consider a population of cells that is both proliferative and motile, and in this context the individual cell based model is stochastic. Here the evolution of the cell density and the position of the free boundary is the net result of a combination of the deterministic motility mechanism and stochastic proliferation events, where the rate of proliferation is taken to be a function of the length of each cell in the stochastic simulations. In all cases considered we study expanding populations where $L(\tau)$ is an increasing function of time.

The key focus of this work is the derivation of a continuum-limit partial differential equations (PDE) description of the individual-based model that provides an accurate description of both the macroscopic density of cells within the domain, as well the movement of the free boundary, $L(\tau)$. We make progress by defining continuous functions by expanding in powers of the small parameter $1/N$, so that, formally, our continuum limit description is accurate in the limit, $N \to \infty$ (Fozard et al., 2009). By carefully neglecting terms of $\mathcal{O}(1/N^2)$, we derive a free boundary problem that describes the spatial and temporal evolution of the cell density within the domain, $0 < x < L(\tau)$, as well as the temporal evolution of the free boundary, $L(\tau)$. We show that our new free boundary condition conserves mass. Comparing averaged data from cell-based simulations with the numerical solution of the continuum limit PDE description of the free boundary problem confirms that the new mass-conserving boundary condition provides an accurate description of the dynamics of the cell-based model across a range of different individual-based mechanisms.

2. A discrete model of cell dynamics in one dimension

In this work, we consider one of the simplest cell-based, off-lattice models of a one-dimensional cross-section of apical surfaces of an epithelial cell population that captures cell-cell adhesion interactions and bulk cellular elasticity. Cells occupy volume and can undergo deformation, neighbouring cells come into contact with each other at node points (Fig. 1), and they interact with each other and the local microenvironment (Murray et al., 2009). We formulate a mathematical description of the dynamics of the cell population using x_i to denote the position of node i (Fig. 1). From Newton's second law of motion

$$m_i \frac{\mathrm{d}^2 x_i}{\mathrm{d}t^2} = \sum_{j \neq i} F^{\mathrm{int}}_{i,j} + F^{\mathrm{visc}}_i, \qquad i = 0, 1, \ldots, N, \tag{1}$$

where $F^{\mathrm{int}}_{i,j}$, the force node j exerts on node i, represents the combined effects of cellular bulk elasticity (leading to crowding and finite size effects) and cell-cell adhesion[1], F^{visc}_i is the viscous force acting on the i^{th} node, and m_i is the mass associated with the i^{th} node.

We now make a number of further assumptions to simplify Eq. (1). Firstly, we assume that cells interact with only their nearest neighbours, so that $F^{\mathrm{int}}_{i,j} = 0$ for $j \neq i \pm 1$, that cells cannot exchange neighbours, and that node zero is pinned at the origin. This entails $0 = x_0(t) < x_1(t) < \ldots < x_{N-1}(t) < x_N(t)$. Secondly, we follow Murray et al. (2009) and assume that the viscous force, F^{visc}_i, which is generated by cell-matrix interactions, is proportional to velocity, $\mathrm{d}x_i/\mathrm{d}t$, with viscosity coefficient η. Thirdly, cells move in dissipative environments, so we assume $m_i \mathrm{d}^2 x_i/\mathrm{d}t^2 = 0$. Finally, we assume the cell population is homogeneous, so that $m_i = m$ for $i = 0, 1, \ldots, N$, and cells respond and generate forces according to the same physical law. As a result, the dynamics of the population can be modelled using the following system of ODEs:

$$x_0(t) = 0; \tag{2}$$

$$\eta \frac{\mathrm{d}x_i}{\mathrm{d}t} = F_{i,i-1} + F_{i,i+1}, \qquad i = 1, \ldots, N-1; \tag{3}$$

$$\eta \frac{\mathrm{d}x_N}{\mathrm{d}t} = F_{N,N-1}. \tag{4}$$

Note that we have suppressed the superscript in $F^{\mathrm{int}}_{i,j}$ for clarity from this point onwards. The system is closed by specifying appropriate initial conditions, $x_i(0) = x_i^0$ for $i = 1, \ldots, N$. To provide a simple exposition, in the initial stages of this work we will assume that cells can be modelled as linear springs; extension to more general cases is provided in Section 4.

3. Linear force law model

We first assume that the interaction force between cells i and $i \pm 1$ can be modelled using a linear force law with constant $k > 0$ and equilibrium length $a > 0$, as in Murray et al. (2009), so that

$$F_{i,i\pm1} = k(a - |x_i - x_{i\pm1}|)\frac{x_i - x_{i\pm1}}{|x_i - x_{i\pm1}|}. \tag{5}$$

Letting $\alpha = k/\eta$ we have

$$x_0(t) = 0, \tag{6}$$

$$\frac{\mathrm{d}x_i}{\mathrm{d}t} = \alpha[x_{i-1} - 2x_i + x_{i+1}], \qquad i = 1, \ldots, N-1, \tag{7}$$

$$\frac{\mathrm{d}x_N}{\mathrm{d}t} = \alpha[x_{N-1} - x_N + a], \tag{8}$$

with initial conditions, $x_i(0) = x_i^0$ for $i = 1, \ldots, N$.

[1] Throughout this work, we will assume $F^{\mathrm{int}}_{i,j} = -F^{\mathrm{int}}_{j,i}$.

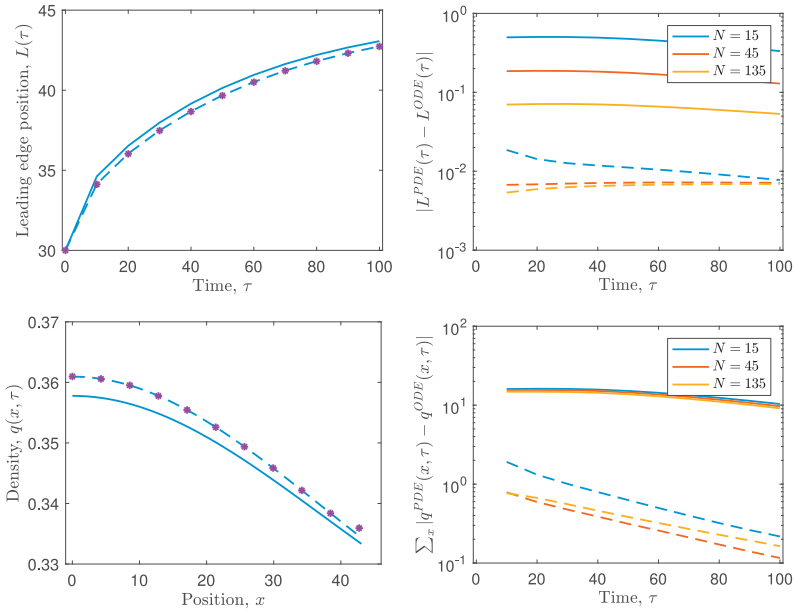

Fig. 2. Comparison of the leading edge position, $L(\tau)$, and cell density, $q(x, \tau)$, predicted by the cell-based model, Eqs. (6)–(8), and the coarse-grained PDE model, Eqs. (29)–(33), as the cell number, N, is varied. In each case, $aN = 45$ and $\alpha/N^2 = 135$ are kept constant. On the left-hand side, the leading edge position, $L(\tau)$, predicted by the cell-based model with $N = 15$ is plotted using purple asterisks, whilst the prediction of the PDE model using the boundary conditions derived in Section 3.1 and stated in Eq. (23) is plotted as a dashed blue line. For comparison, the leading edge position predicted using the boundary conditions of Murray et al. (2009) is plotted as a solid blue line. On the right-hand side, the error in the predictions of the coarse-grained model are shown for both the boundary conditions stated in Eq. (23) (dashed lines), and those derived by Murray et al. (2009) (solid lines), for a range of values of cell number, N. (For interpretation of the references to colour in this figure legend, the reader is referred to the web version of this article.)

Eqs. (6)–(8) can be solved analytically. However, since in this work our aim is to extend to more general (analytically intractable) cases where nonlinear force terms are used to model cellular dynamics, we solve for the position of each node, x_i, numerically using a simple forward Euler method with time-step $\Delta t = 0.001$. Exemplar results for the model are shown in Fig. 2, where we demonstrate how the leading edge and cell density of an initially compressed population of cells evolves over time.

3.1. Continuum approximation

To make progress in deriving an equivalent continuum, coarse-grained model, with a slight abuse of notation[2] we will extend node position, $x_i(t)$, which is only defined for discrete $i \in \{0, \ldots, N\}$, to a smooth function, $x(i, t)$, which is defined for $i \in [0, N]$. The function $x(i, t)$ will approximate x_i when i is an integer:

$$x_i(t) \approx x(i, t), \qquad i = 0, 1, \ldots, N. \tag{9}$$

To facilitate coarse graining, we first non-dimensionalise the model specified in Eqs. (6)–(8) using the scalings

$$\tilde{i} = \frac{i}{N}, \qquad \tilde{x} = \frac{x}{aN}, \qquad \tilde{t} = \frac{\alpha t}{N^2} = \frac{kt}{\eta N^2}, \tag{10}$$

so that $\tilde{i} \in \{0, 1/N, 2/N, \ldots, 1\}$ and $\tilde{x} \sim \mathcal{O}(1)$. The model equations are then

$$\tilde{x}(0, \tilde{t}) = 0, \tag{11}$$

$$\frac{\partial \tilde{x}(\tilde{i}, \tilde{t})}{\partial \tilde{t}} = N^2\left[\tilde{x}(\tilde{i} - 1/N, \tilde{t}) - 2\tilde{x}(\tilde{i}, \tilde{t}) + \tilde{x}(\tilde{i} + 1/N, \tilde{t})\right], \tag{12}$$

$$\frac{\partial \tilde{x}(1, \tilde{t})}{\partial t} = N^2\left[\tilde{x}(1 - 1/N, \tilde{t}) - \tilde{x}(1, \tilde{t}) + 1/N\right], \tag{13}$$

where Eq. (12) holds for $\tilde{i} = 1/N, \ldots, 1 - 1/N$, and we have corresponding initial conditions of the form $\tilde{x}(\tilde{i}, 0) = \tilde{x}_i^0$ for $i = 1/N, \ldots, 1$.

Performing a Taylor expansion about $\tilde{i}$ within Eq. (12) gives, on neglecting terms that are $\mathcal{O}\left(1/N^2\right)$,

$$\frac{\partial \tilde{x}}{\partial \tilde{t}} = \frac{\partial^2 \tilde{x}}{\partial \tilde{i}^2}, \qquad \tilde{i} \in (0, 1). \tag{14}$$

The left-hand boundary condition is simply $\tilde{x}(0, \tilde{t}) = 0$. To derive the right-hand boundary condition, we again Taylor expand and neglect terms that are $\mathcal{O}\left(1/N^2\right)$ to give, at $\tilde{i} = 1$,

$$\begin{aligned} \frac{1}{N}\frac{\partial \tilde{x}}{\partial \tilde{i}} &= N\left[\tilde{x} - \frac{1}{N}\frac{\partial \tilde{x}}{\partial \tilde{i}} + \frac{1}{2N^2}\frac{\partial^2 \tilde{x}}{\partial \tilde{i}^2} + \ldots - \tilde{x} + \frac{1}{N}\right] \\ &= 1 - \frac{\partial \tilde{x}}{\partial \tilde{i}} + \frac{1}{2N}\frac{\partial^2 \tilde{x}}{\partial \tilde{i}^2}. \end{aligned} \tag{15}$$

In terms of the dimensional variables, the coarse-grained model is therefore

$$\frac{\partial x}{\partial t} = \alpha \frac{\partial^2 x}{\partial i^2}, \qquad i \in (0, N), \tag{16}$$

with boundary conditions

$$x(0, t) = 0 \qquad \text{and} \qquad \left.\frac{\partial x}{\partial t}\right|_{i=N} = \alpha\left[a - \frac{\partial x}{\partial i} + \frac{1}{2}\frac{\partial^2 x}{\partial i^2}\right]\Bigg|_{i=N}. \tag{17}$$

Initial conditions can be specified by extending the discrete initial conditions, $x_i(0) = x_i^0$ for $i = 1, \ldots, N$, to a continuous function $x(i, 0)$ such that $x(i, 0) = x_i^0$ for $i = 1, \ldots, N$. Throughout this work, for simplicity we extend the discrete initial condition to a piecewise linear continuous function.

[2] Note that $x(i, t)$ is a continuous variable representing position, has dimensions of length, and ranges between 0 and $N \times a$ when cells are at equilibrium.

3.2. Derivation of the corresponding cell density model

Cell density per unit length, $q(x, t)$, can be defined implicitly using the relation

$$i(x,t) = \int_0^x q(y,t)\,\mathrm{d}y, \tag{18}$$

where i is the cell index. This equation describes the fact that the position of node index i depends on the cell density to the left of the node. Eq. (18) is equivalent to $q(x,t) = \partial i(x,t)/\partial x$, and it ensures $i = 0$ at the left-hand boundary, $x = 0$. To reformulate Eqs. (16) and (17) in terms of variation in cell density with position, x, and time, t, we follow (Murray et al., 2009) and perform a change of variables from (i, t) to (x, τ) where i and x are related through Eq. (18) and $t = \tau$.

Noting that

$$\begin{pmatrix} \left.\frac{\partial x}{\partial i}\right|_t & \left.\frac{\partial x}{\partial t}\right|_i \\ \left.\frac{\partial \tau}{\partial i}\right|_t & \left.\frac{\partial \tau}{\partial t}\right|_i \end{pmatrix} = \begin{pmatrix} \left.\frac{\partial i}{\partial x}\right|_\tau & \left.\frac{\partial i}{\partial \tau}\right|_x \\ \left.\frac{\partial t}{\partial x}\right|_\tau & \left.\frac{\partial t}{\partial \tau}\right|_x \end{pmatrix}^{-1} = \frac{1}{\left.\frac{\partial i}{\partial x}\right|_\tau \left.\frac{\partial t}{\partial \tau}\right|_x - \left.\frac{\partial i}{\partial \tau}\right|_x \left.\frac{\partial t}{\partial x}\right|_\tau} \begin{pmatrix} \left.\frac{\partial t}{\partial \tau}\right|_x & -\left.\frac{\partial i}{\partial \tau}\right|_x \\ -\left.\frac{\partial t}{\partial x}\right|_\tau & \left.\frac{\partial i}{\partial x}\right|_\tau \end{pmatrix},$$

we have

$$\frac{\partial x}{\partial i} = \left(\frac{\partial i}{\partial x}\right)^{-1} = \frac{1}{q}, \tag{19}$$

$$\frac{\partial x}{\partial t} = -\left(\frac{\partial i}{\partial x}\right)^{-1} \frac{\partial i}{\partial \tau} = -\frac{1}{q}\frac{\partial i}{\partial \tau}. \tag{20}$$

Substituting Eqs. (19) and (20) into the right-hand side of Eq. (16) gives

$$\frac{\partial x}{\partial \tau} = -\frac{\alpha}{q^3}\frac{\partial q}{\partial x}, \qquad x \in [0, L(\tau)]. \tag{21}$$

Eq. (21) is the characteristic equation and it represents how the domain evolves over time through tracking constant node index, i. After rearrangement, multiplying by q and differentiating with respect to x, we have

$$\frac{\partial q}{\partial \tau} = \frac{\partial}{\partial x}\left(\frac{\alpha}{q^2}\frac{\partial q}{\partial x}\right), \qquad x \in (0, L(\tau)). \tag{22}$$

The same change of variables applied to the boundary conditions in Eq. (17) yields[3]

$$\left.\frac{\partial q}{\partial x}\right|_{x=0} = 0 \qquad \text{and} \qquad \left(\frac{1}{2q^2}\frac{\partial q}{\partial x} + aq - 1\right)\Big|_{x=L(\tau)} = 0. \tag{23}$$

As a check on the validity of the derived boundary conditions, we note that the system must conserve total cell density, *i.e.*

$$\frac{\mathrm{d}}{\mathrm{d}\tau}\int_0^{L(\tau)} q(x,\tau)\,\mathrm{d}x = 0. \tag{24}$$

Evaluating the above expression gives (again, using the characteristic Eq. (21))

$$\begin{aligned} \frac{\mathrm{d}}{\mathrm{d}\tau}\int_0^{L(\tau)} q(x,\tau)\,\mathrm{d}x &= \frac{\mathrm{d}L(\tau)}{\mathrm{d}\tau}q(L(\tau),\tau) + \int_0^{L(\tau)} \frac{\partial q}{\partial \tau}(x,\tau)\,\mathrm{d}x \\ &= \frac{\mathrm{d}L(\tau)}{\mathrm{d}\tau}q(L(\tau),\tau) + \int_0^{L(\tau)} \frac{\partial}{\partial x}\left[\frac{\alpha}{q^2}\frac{\partial q}{\partial x}\right]\mathrm{d}x \\ &= \left[-\frac{\alpha}{q^3}\frac{\partial q}{\partial x}q + \frac{\alpha}{q^2}\frac{\partial q}{\partial x}\right]\Big|_{x=L(\tau)} - \left.\frac{\alpha}{q^2}\frac{\partial q}{\partial x}\right|_{x=0} \\ &= 0. \end{aligned} \tag{25}$$

Therefore total density is conserved using the derived boundary conditions. Note that the boundary condition applied at the free, right-hand boundary, $L(\tau)$, is slightly different to that derived in Murray et al. (2009), where the boundary condition was derived by neglecting terms that are $\mathcal{O}(1/N)$ and is of the form $q = 1/a$ for $x = L(\tau)$.

To establish initial conditions, we use Eq. (18) together with a finite difference approximation to write

$$\begin{aligned} 2 &= (i+1) - (i-1) \\ &= \int_{x_{i-1}^0}^{x_{i+1}^0} q(x,0)\mathrm{d}x \approx \left(x_{i+1}^0 - x_{i-1}^0\right) q_0\left(x_i^0\right), \quad i = 1, \ldots, N-1, \end{aligned} \tag{26}$$

which can be rearranged to give

$$q_0\left(x_i^0\right) = \frac{2}{x_{i+1}^0 - x_{i-1}^0}, \qquad i = 1, \ldots, N-1. \tag{27}$$

A similar finite difference approximation applied at the left- and right-hand boundaries gives

$$q_0(0) = \frac{1}{x_1^0} \qquad \text{and} \qquad q_0(x_N^0) = \frac{1}{x_N^0 - x_{N-1}^0}. \tag{28}$$

We treat $q_0(x)$ as piecewise linear between node positions.

3.2.1. Numerical solution

In summary, the coarse-grained model consists of a PDE for the evolution of cell density

$$\frac{\partial q}{\partial \tau} = \frac{\partial}{\partial x}\left(\frac{\alpha}{q^2}\frac{\partial q}{\partial x}\right), \qquad x \in (0, L(\tau)), \tag{29}$$

together with boundary conditions

$$\left.\frac{\partial q}{\partial x}\right|_{x=0} = 0 \qquad \text{and} \qquad \left(\frac{1}{2q^2}\frac{\partial q}{\partial x} + aq - 1\right)\Big|_{x=L(\tau)} = 0, \tag{30}$$

and initial condition

$$q(x,0) = q_0(x), \qquad x \in (0, L(0)). \tag{31}$$

The characteristic equation is

$$\frac{\partial x}{\partial \tau} = -\frac{\alpha}{q^3}\frac{\partial q}{\partial x}, \qquad x \in [0, L(\tau)], \tag{32}$$

and we can use the characteristics to specify the evolution of the domain with time. In particular, we have

$$\frac{\mathrm{d}L(\tau)}{\mathrm{d}\tau} = \left(-\frac{\alpha}{q^3}\frac{\partial q}{\partial x}\right)\Big|_{L(\tau)}. \tag{33}$$

In order to solve Eqs. (29)–(33) numerically we employ a Lagrangian transformation to map the free boundary problem to a fixed domain. We let $\tau = T$ and

$$\begin{aligned} &x = \Gamma(X,T) \qquad \text{with} \qquad X = \Gamma(X,0), \qquad 0 = \Gamma(0,T), \\ &L(T) = \Gamma(L(0),T), \end{aligned} \tag{34}$$

so that

$$\frac{\partial}{\partial x} = \frac{1}{\Gamma_X}\frac{\partial}{\partial X} \qquad \text{and} \qquad \frac{\partial}{\partial \tau} = \frac{\partial}{\partial T} - \frac{1}{\Gamma_X}\frac{\partial \Gamma}{\partial T}\frac{\partial}{\partial T}, \tag{35}$$

[3] Note that the boundary condition at $x = L(\tau)$ is derived using the characteristic Eq. (21), see Appendix A for more details.

where we have adopted the notation $\partial\Gamma/\partial X = \Gamma_X$. Substitution into equations Eqs. (29) and (33) yields equations for evolution of the domain and the density therein:

$$\frac{\partial \Gamma}{\partial T} = -\frac{\alpha}{q^3}\frac{1}{\Gamma_X}\frac{\partial q}{\partial X}, \qquad X \in (0, L(0)); \tag{36}$$

$$\frac{\partial q}{\partial T} - \frac{1}{\Gamma_X}\frac{\partial \Gamma}{\partial T}\frac{\partial q}{\partial X} = \frac{1}{\Gamma_X}\frac{\partial}{\partial X}\left(\frac{\alpha}{q^2}\frac{1}{\Gamma_X}\frac{\partial q}{\partial X}\right), \qquad X \in (0, L(0)). \tag{37}$$

The initial and boundary conditions for $\Gamma(X, T)$ are specified in Eq. (34), and for $q(X, T)$ we have

$$\left.\frac{\partial q}{\partial X}\right|_{X=0} = 0 \qquad \text{and} \qquad \left.\left(\frac{1}{2q^2}\frac{1}{\Gamma_X}\frac{\partial q}{\partial X} + aq - 1\right)\right|_{X=L(0)} = 0, \tag{38}$$

together with

$$q(X, 0) = q_0(X) \qquad X \in (0, L(0)). \tag{39}$$

We solve the model numerically using an implicit finite difference method with Picard iteration. Full details are given in Appendix B.

3.3. Results

The coarse-grained PDE model is very accurate in its prediction of both evolution of the cell density, $q(x, \tau)$, and the free boundary at $x = L(\tau)$ (see Fig. 2), even for relatively low cell numbers (here we show results for cell numbers as low as $N = 15$). The accuracy of the PDE model increases as the cell number, N, increases; this is in line with expectations since the error of the coarse-grained PDE model is $\mathcal{O}(1/N^2)$. To ensure sensible comparisons, the results in Fig. 2 were generated by initialising N cells with equal lengths in the interval $x \in (0, 30)$ and varying the model parameters such that $\alpha = 15(N/45)^2$ and $a = 45/N$. This choice ensures that the scalings for x and τ do not change with increasing N. In each case, cells are initially compressed but will eventually expand to fill the domain $x \in (0, 45)$.

We also compare the results of our model against those derived in Murray et al. (2009), where the boundary condition at the free boundary was derived by neglecting terms $\mathcal{O}(1/N)$ and is of the form $q = 1/a$ for $x = L(\tau)$. As expected, the boundary condition derived here leads to a more accurate prediction of the dynamics of the cell-based model because we neglect only terms that are $\mathcal{O}(1/N^2)$ rather than $\mathcal{O}(1/N)$.

4. General force law model

In this section we follow the work of Murray et al. (2012) and generalise the 1D cell-based model to account for a more general force law, $F_{i,\,i\pm1}$, between neighbouring nodes, i and $i \pm 1$, in Eqs. (2)–(4). For concreteness, in our examples we will work with a force law of the form (Murray et al., 2012)

$$F_{i,i\pm1} = F(|x_i - x_{i\pm1}|)\frac{x_i - x_{i\pm1}}{|x_i - x_{i\pm1}|} = k(a - |x_i - x_{i\pm1}|)^n \frac{x_i - x_{i\pm1}}{|x_i - x_{i\pm1}|}, \tag{40}$$

for some real valued exponent, n, where $n = 1$ gives a linear force law, as considered in Section 3, $n = 3$ gives a cubic force law, and $n = 3/2$ gives the Hertz force law (see Fig. 3). These force laws are chosen to cover a wide range of potential cell interactions and / or represent different mechanical properties of cells. The nodes evolve over time according to

$$x_0(t) = 0, \tag{41}$$

$$\eta\frac{\mathrm{d}x_i}{\mathrm{d}t} = F(x_i - x_{i-1}) - F(x_{i+1} - x_i), \qquad i = 1, \ldots, N-1, \tag{42}$$

$$\eta\frac{\mathrm{d}x_N}{\mathrm{d}t} = F(x_N - x_{N-1}), \tag{43}$$

where $F(x) = k(a - x)^n$. The initial conditions are $x_i(0) = x_i^0$ for $i = 1, \ldots, N$. As for the linear force law case, we solve for the position of each node, x_i, numerically using a simple forward Euler method with time-step $\Delta t = 0.001$. Exemplar results for the model are shown in Fig. 4, where we show how the leading edge and cell density of an initially compressed population of cells evolves over time for the three different force laws.

4.1. Continuum approximation

To derive a coarse-grained model we again, with a slight abuse of notation, extend node positions, $x_i(t)$, to a smooth function $x(i, t)$, for $i \in [0, N]$, and non-dimensionalise Eqs. (41)–(43) using similar scalings to the simple linear case,

$$\tilde{i} = \frac{i}{N}, \qquad \tilde{x} = \frac{x}{aN}, \qquad \tilde{t} = \frac{\alpha a^{n-1}t}{N^2} = \frac{ka^{n-1}t}{\eta N^2},$$

so that $\tilde{i} \sim \mathcal{O}(1)$ and $\tilde{x} \sim \mathcal{O}(1)$. We also define the non-dimensional force function to be

$$\tilde{F}(\cdot) = (1 - \cdot)^n. \tag{44}$$

To derive an equivalent coarse-grained continuum model we proceed as in Section 3.1, performing a Taylor expansion about $\tilde{i}$ within the non-dimensionalised system to give, on neglecting terms which are $\mathcal{O}(1/N^2)$,

$$\frac{\partial \tilde{x}}{\partial \tilde{t}} = -\tilde{F}'\left(\frac{\partial \tilde{x}}{\partial \tilde{i}}\right)\frac{\partial^2 \tilde{x}}{\partial \tilde{i}^2}, \qquad \tilde{i} \in (0, 1). \tag{45}$$

The left-hand boundary condition remains as $\tilde{x}(0, \tilde{t}) = 0$ and, as before, to derive the right-hand boundary condition we Taylor expand and neglect terms which are $\mathcal{O}(1/N^2)$ to give, at $\tilde{i} = 1$,

$$\frac{1}{N}\frac{\partial \tilde{x}}{\partial \tilde{t}} = \tilde{F}\left(\frac{\partial \tilde{x}}{\partial \tilde{i}}\right) - \frac{1}{2N}\tilde{F}'\left(\frac{\partial \tilde{x}}{\partial \tilde{i}}\right)\frac{\partial^2 \tilde{x}}{\partial \tilde{i}^2}. \tag{46}$$

Rewriting in terms of dimensional variables we have the following PDE for $x(i, t)$:

$$\eta\frac{\partial x}{\partial t} = -F'\left(\frac{\partial x}{\partial i}\right)\frac{\partial^2 x}{\partial i^2}, \qquad i \in (0, N). \tag{47}$$

The boundary conditions are

$$x(0, t) = 0 \quad \text{and} \quad \eta\left.\frac{\partial x}{\partial t}\right|_{i=N} = \left.\left[F\left(\frac{\partial x}{\partial i}\right) - \frac{1}{2}\frac{\partial^2 x}{\partial i^2}F'\left(\frac{\partial x}{\partial i}\right)\right]\right|_{i=N}. \tag{48}$$

As before, the initial conditions can be specified by extending the discrete initial conditions, $x_i(0) = x_i^0$ for $i = 1, \ldots, N$, to a continuous function $x(i, 0)$ such that $x(i, 0) = x_i^0$ for $i = 1, \ldots, N$. As a consistency check, we note that when $n = 1$, as for the linear force law, Eqs. (47) and (48) reduce to Eqs. (16) and (17).

4.2. Derivation of the corresponding cell density model

We can establish a PDE describing the evolution of cell density with position, x, and time, t, by making the same change of variables as in Section 3.2. Following a simple substitution of terms from Eqs. (19) and (20) into Eq. (47) we obtain the PDE

$$\eta\frac{\partial x}{\partial \tau} = \frac{1}{q^3}F'\left(\frac{1}{q}\right)\frac{\partial q}{\partial x}, \qquad x \in [0, L(\tau)], \tag{49}$$

Force model	Force law, $F(x)$	Diffusion term, $D(q)$
Linear $(n = 1)$	$k(a - x)$	$\frac{\alpha}{q^2}$
Cubic $(n = 3)$	$k(a - x)^3$	$\frac{3\alpha}{q^2}\left(a - \frac{1}{q}\right)^2$
Hertz $(n = 3/2)$	$k(a - x)^{3/2}$	$\frac{3\alpha}{2q^2}\left(a - \frac{1}{q}\right)^{1/2}$

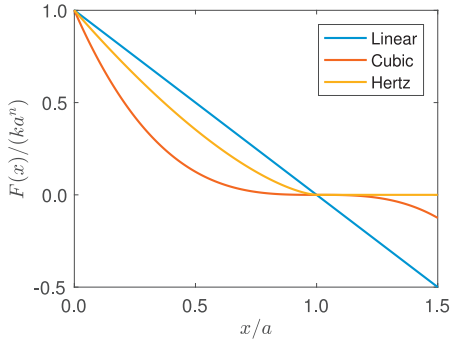

Fig. 3. The force laws, $F(x)$, and the corresponding diffusion coefficient, $D(q)$, considered in Section 4.1.

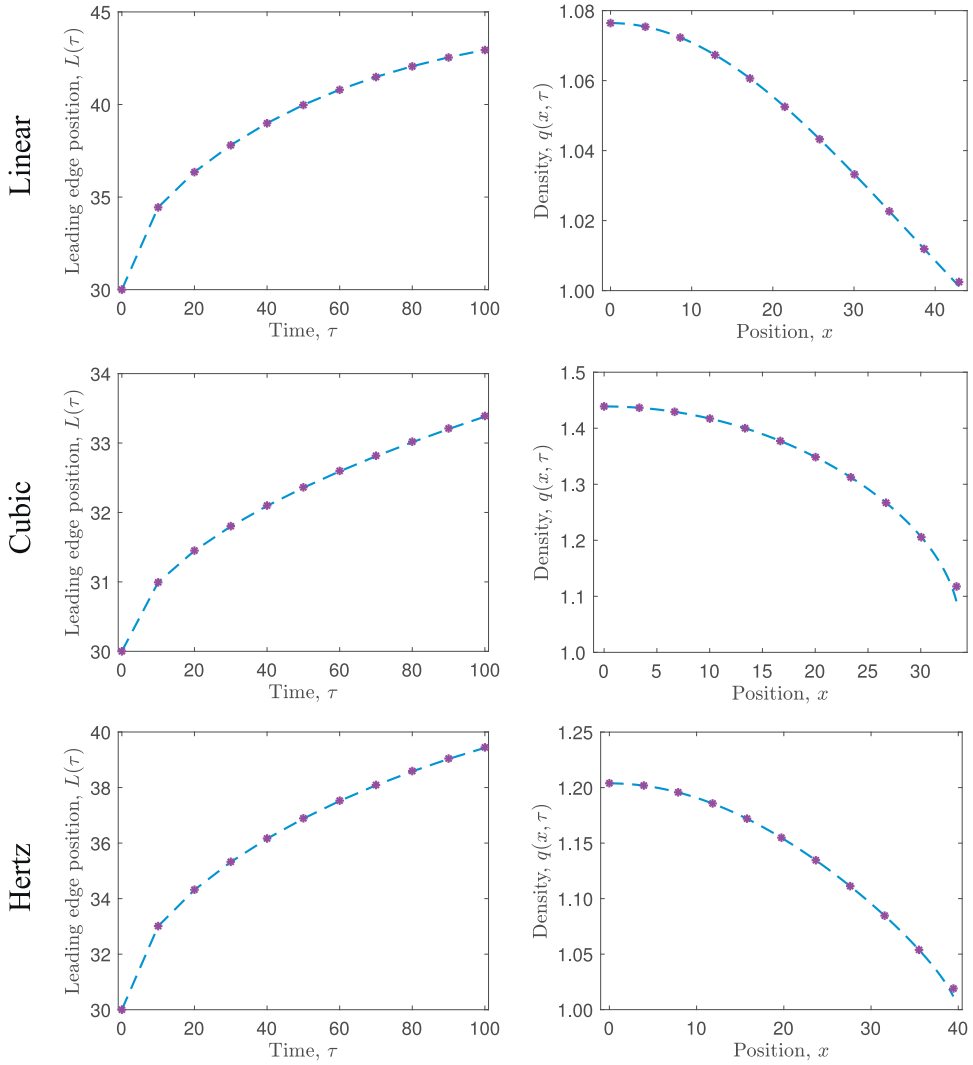

Fig. 4. Comparison of the leading edge position, $L(\tau)$, and cell density, $q(x, \tau)$, predicted by the cell-based model, Eqs. (41)–(43) with the force law as defined in (40) (purple asterisks), and the coarse-grained PDE model, Eq. (55)–(59) (blue dashed line), as the force law is varied (see Fig. 3). In each case, $N = 45$ cells are initialised uniformly in $x \in (0, 30)$, and $aN = 45$ and $\alpha/a^{1-n}N^2 = 135$ are fixed. (For interpretation of the references to colour in this figure legend, the reader is referred to the web version of this article.)

which represents how the domain, x, evolves along characteristics with constant index. Substitution of Eqs. (19) and (20), and a simple rearrangement (multiplying by q and differentiating with respect to x, identical to earlier arguments), results in a PDE for the cell density of the form

$$\frac{\partial q}{\partial \tau} = \frac{\partial}{\partial x}\left(D(q)\frac{\partial q}{\partial x}\right), \qquad x \in (0, L(\tau)), \tag{50}$$

where the diffusion coefficient, $D(q)$, is defined as

$$D(q) = -\frac{1}{\eta q^2}F'\left(\frac{1}{q}\right). \tag{51}$$

The characteristic Eq. (49) can then be rewritten as

$$\frac{\partial x}{\partial \tau} = -\frac{1}{q}D(q)\frac{\partial q}{\partial x}, \qquad x \in [0, L(\tau)]. \tag{52}$$

Under the same change of variables, boundary conditions become

$$\left.\frac{\partial q}{\partial x}\right|_{x=0} = 0 \qquad \text{and} \qquad \left.\left(\frac{1}{\eta}F\left(\frac{1}{q}\right) + \frac{1}{2q}D(q)\frac{\partial q}{\partial x}\right)\right|_{x=L(\tau)} = 0. \tag{53}$$

As in Section 3.2, we note that the system conserves total cell density:

$$\begin{aligned}\frac{\mathrm{d}}{\mathrm{d}\tau}\int_0^{L(\tau)} q(x,\tau)\,\mathrm{d}x &= \frac{\mathrm{d}L(\tau)}{\mathrm{d}\tau}q(L(\tau),\tau) + \int_0^{L(\tau)}\frac{\partial q}{\partial \tau}(x,\tau)\,\mathrm{d}x \\ &= \frac{\mathrm{d}L(\tau)}{\mathrm{d}\tau}q(L(\tau),\tau) + \int_0^{L(\tau)}\frac{\partial}{\partial x}\left[D(q)\frac{\partial q}{\partial x}\right]\mathrm{d}x \\ &= \left[-\frac{1}{q}D(q)\frac{\partial q}{\partial x}q + D(q)\frac{\partial q}{\partial x}\right]\Bigg|_{x=L(\tau)} - D(q)\frac{\partial q}{\partial x}\Bigg|_{x=0} \\ &= 0,\end{aligned} \tag{54}$$

where the final result is established using Eq. (52).

4.2.1. Numerical solution

In summary, the coarse-grained model consists of a PDE for the evolution of cell density,

$$\frac{\partial q}{\partial \tau} = \frac{\partial}{\partial x}\left[D(q)\frac{\partial q}{\partial x}\right], \qquad x \in (0, L(\tau)), \tag{55}$$

together with the boundary conditions

$$\left.\frac{\partial q}{\partial x}\right|_{x=0} = 0 \qquad \text{and} \qquad \left.\left[\frac{1}{\eta}F\left(\frac{1}{q}\right) + \frac{D(q)}{2q}\frac{\partial q}{\partial x}\right]\right|_{x=L(\tau)} = 0, \tag{56}$$

and initial condition

$$q(x,0) = q_0(x), \qquad x \in (0, L(0)). \tag{57}$$

The characteristic equation is

$$\frac{\partial x}{\partial \tau} = -\frac{1}{q}D(q)\frac{\partial q}{\partial x}. \qquad x \in [0, L(\tau)], \tag{58}$$

and we can use it to specify the evolution of the domain with time. In particular, we have

$$\frac{\mathrm{d}L(\tau)}{\mathrm{d}\tau} = \left.\left(-\frac{1}{q}D(q)\frac{\partial q}{\partial x}\right)\right|_{L(\tau)}. \tag{59}$$

As in Section 3.2.1, in order to solve the coarse-grained model numerically, we employ a Lagrangian transformation to map the free boundary problem to a fixed domain: we let $\tau = T$ and

$$x = \Gamma(X,T) \qquad \text{with} \qquad X = \Gamma(X,0),$$

$$0 = \Gamma(0,T), \qquad L(T) = \Gamma(L(0),T), \tag{60}$$

to give

$$\frac{\partial \Gamma}{\partial T} = -\frac{D(q)}{q\Gamma_X}\frac{\partial q}{\partial X}, \qquad X \in (0, L(0)), \tag{61}$$

$$\frac{\partial q}{\partial T} - \frac{1}{\Gamma_X}\frac{\partial \Gamma}{\partial T}\frac{\partial q}{\partial X} = \frac{1}{\Gamma_X}\frac{\partial}{\partial X}\left(\frac{D(q)}{\Gamma_X}\frac{\partial q}{\partial X}\right), \qquad X \in (0, L(0)). \tag{62}$$

The initial and boundary conditions for $\Gamma(X, T)$ are specified in Eq. (34), and for $q(X, T)$ we have

$$\left.\frac{\partial q}{\partial X}\right|_{X=0} = 0 \qquad \text{and} \qquad \left.\left[\frac{1}{\eta}F\left(\frac{1}{q}\right) + \frac{D(q)}{2q\Gamma_X}\frac{\partial q}{\partial X}\right]\right|_{X=L(0)} = 0, \tag{63}$$

together with

$$q(X,0) = q_0(X) \qquad X \in (0, L(0)). \tag{64}$$

We solve the model numerically using an implicit finite difference method with Picard iteration. Full details are given in Appendix B.

4.3. Results

Across all force laws tested, the coarse-grained PDE model is very accurate in its prediction of both evolution of the cell density, $q(x, \tau)$, and the free boundary at $x = L(\tau)$ (see Fig. 4). The only minor deviation in the predictions of the models is found at the leading edge, where the gradient in the cell density is largest. Note that in this region the approximation of the density in the cell-based model is lower order in N, so this deviation could perhaps be reasonably expected.

5. Introducing proliferation into the model

In this section, we extend the model to include proliferation. The mechanism that we incorporate is stochastic, with each cell dividing with a defined rate per unit time. We derive a coarse-grained PDE model to describe the evolution of the domain, and cell density therein, over time, and demonstrate the validity of the coarse-grained model by comparing its solution to averaged results from the cell-based model.

5.1. Proliferation mechanism

To extend the model to include proliferation, we assume that each cell proliferates stochastically at a rate per unit time that is a function of its length. That is, the probability that cell i divides in the time interval $[t, t + \mathrm{d}t)$ is $G_i\mathrm{d}t$ where $G_i = G(|x_i - x_{i-1}|)$. When a cell proliferates, a new node is introduced at its centre to establish the daughter cells, and we relabel the node indices to ensure their order, that is, $x_i(t) < x_{i+1}(t)$ for $i = 0, \ldots, N(t)$ and $t \geq 0$. Subsequently, when a new node (and cell) is introduced due to the proliferation of the i^{th} cell, we relabel the nodes with indices $j = i + 1, \ldots, N$ using $j \mapsto j + 1$, as shown in Fig. 5. In this work, we explore the dynamics introduced by three different types of proliferation mechanism: (i) cells proliferate at constant rate; (ii) cells proliferate at rate proportional to their length; and (iii) cells are more likely to proliferate as they approach a target length. Specific functional forms for the proliferation rates we consider in this work are provided in Fig. 6.

To generate individual realisations of this discrete stochastic model we use a constant time-step algorithm, with time-step $\Delta t = 0.001$. At each step, we first update the position of each node, x_i, $i = 1, \ldots, N$, by using a simple forward Euler method to integrate Eqs. (41)–(43) numerically, then we check to see whether a cell proliferation event occurs (and, if so, which cell proliferates). A cell

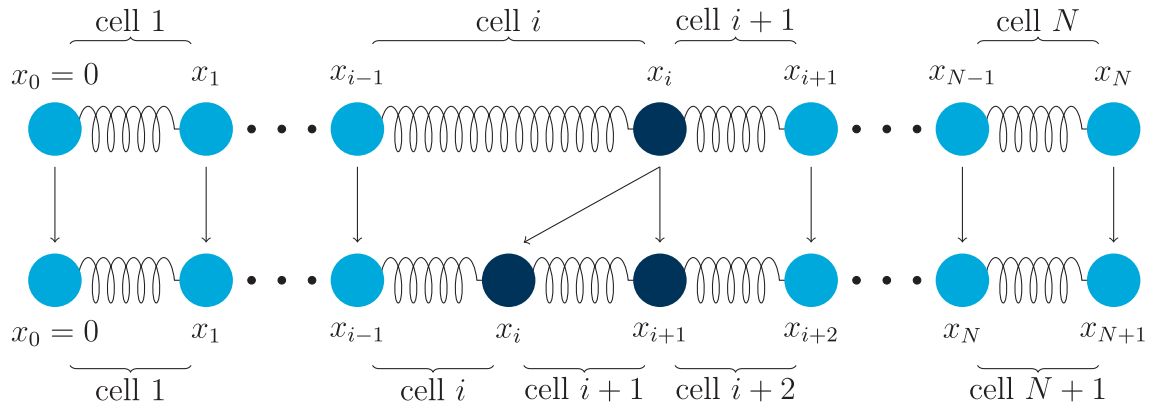

Fig. 5. Proliferation of cell i entails the introduction of a new node at the cell centre, and relevant nodes and cells are then relabelled to ensure $x_j < x_{j+1}$ for $j \in \{0, 1, \ldots, N\}$.

Proliferation	Proliferation law ($G(x)$)
Constant	β
Linear	$\dfrac{\beta x}{a}$
Hyperbolic	$\beta\left[\tanh\left(4\left(x-\dfrac{3a}{4}\right)\right)+\dfrac{1}{2}\right]$

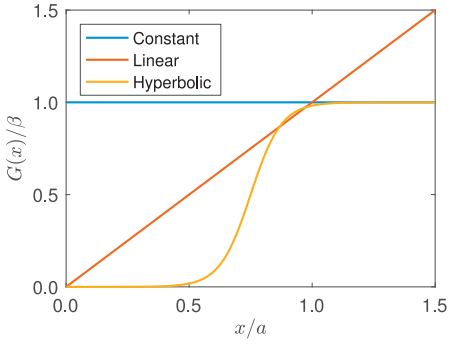

Fig. 6. The proliferation laws considered in Section 5. Here, as before, the natural cell length is a, and β represents the intrinsic proliferation rate.

proliferation event occurs with probability $\sum_{j=0}^{N} G_j \Delta t$ and, given a cell proliferation event occurs, the probability that cell i proliferates is $G_i / \sum_{j=0}^{N} G_j$, $i = 1, \ldots, N$. In each case, we use rejection sampling to implement the decision (Gelman et al., 2013), and if a cell proliferation occurs, we update the node indices as indicated in Fig. 5. Note that this algorithm enforces the condition that at most one cell can proliferate per time-step; this is a reasonable approximation for the parameters used in this work.

5.2. Derivation of cell density model with proliferation

As the proliferation mechanism we have introduced is stochastic, we now consider evolution of the expected positions of the nodes over time. We make progress by considering the system over an infinitesimally small time interval $[t, t+\mathrm{d}t)$ and condition whether cell proliferation takes place during that time interval. The position of each node after a small time interval will depend on if and where cell proliferation occurs and the resulting forces exerted by neighbouring cells. We write, for $i = 1, \ldots, N-1$,

$$
\begin{aligned}
x_i^N(t+\mathrm{d}t) = {} & \left(x_i^N(t) + \mathrm{d}t\,\frac{F_{i,i-1}^N - F_{i,i+1}^N}{\eta}\right) \\
& \times \mathbb{1}\{\text{no proliferation in } [t, t+\mathrm{d}t)\} \\
& \left(x_i^{N-1}(t) + \mathrm{d}t\,\frac{F_{i,i-1}^{N-1} - F_{i,i+1}^{N-1}}{\eta}\right) \\
& \times \mathbb{1}\{\text{proliferation to the right of cell } i \text{ in } [t, t+\mathrm{d}t)\} \\
& + \frac{1}{2}\left[\left(x_i^{N-1}(t) + \mathrm{d}t\,\frac{F_{i,i-1}^{N-1} - F_{i,i+1}^{N-1}}{\eta}\right)\right. \\
& \left. + \left(x_{i-1}^{N-1}(t) + \mathrm{d}t\,\frac{F_{i-1,i-2}^{N-1} - F_{i-1,i}^{N-1}}{\eta}\right)\right] \\
& \times \mathbb{1}\{\text{proliferation of cell } i \text{ in } [t, t+\mathrm{d}t)\} \\
& + \left(x_{i-1}^{N-1}(t) + \mathrm{d}t\,\frac{F_{i-1,i-2}^{N-1} - F_{i-1,i}^{N-1}}{\eta}\right) \\
& \times \mathbb{1}\{\text{proliferation to the left of cell } i \text{ in } [t, t+\mathrm{d}t)\} \\
& + (\text{position of cell } i \text{ if more than one proliferation event in } [t, t+\mathrm{d}t)) \\
& \times \mathbb{1}\Big\{\text{more than one cell proliferation event in} [t, t+\mathrm{d}t)\Big\},
\end{aligned}
\tag{65}
$$

and

$$
\begin{aligned}
x_N^N(t+\mathrm{d}t) = {} & \left(x_N^N(t) + \mathrm{d}t\,\frac{F_{N,N-1}^N}{\eta}\right) \\
& \times \mathbb{1}\{\text{no proliferation in } [t, t+\mathrm{d}t)\} \\
& \left(x_N^{N-1}(t) + \mathrm{d}t\,\frac{F_{N,N-1}^{N-1}}{\eta}\right) \\
& \times \mathbb{1}\{\text{proliferation to the right of cell } N \text{ in } [t, t+\mathrm{d}t)\} \\
& + \frac{1}{2}\left[\left(x_N^{N-1}(t) + \mathrm{d}t\,\frac{F_{N,N-1}^{N-1}}{\eta}\right)\right. \\
& \left. + \left(x_{N-1}^{N-1}(t) + \mathrm{d}t\,\frac{F_{N-1,N-2}^{N-1} - F_{N-1,N}^{N-1}}{\eta}\right)\right] \\
& \times \mathbb{1}\{\text{proliferation of cell } N \text{ in } [t, t+\mathrm{d}t)\}
\end{aligned}
$$

$$+\left(x_{N-1}^{N-1}(t)+\mathrm{d}t\,\frac{F_{N-1,N-2}^{N-1}-F_{N-1,N}^{N-1}}{\eta}\right)$$
$$\times\mathbb{1}\{\text{proliferation to the left of cell } N \text{ in } [t,t+\mathrm{d}t)\}$$
$$+\Big(\text{position of cell } N \text{ if more than one proliferation event in } [t,t+\mathrm{d}t)\Big)$$
$$\times\mathbb{1}\Big\{\text{more than one cell proliferation event in } [t,t+\mathrm{d}t)\Big\}. \tag{66}$$

In Eqs. (65) and (66) and $\mathbb{1}$ is the indicator function and $X_i^N(t)$ is the position of cell i at time t when there are N cells. The superscript N on the force terms, $F_{i,j}$, indicate that they are evaluated using the positions of cells i and j when there are N cells.

The required probabilities to specify the indicator functions are

$$\mathbb{P}(\text{no proliferation in } [t,t+\mathrm{d}t)) = 1-\mathrm{d}t\sum_{j=1}^{N}G\big(x_j-x_{j-1}\big), \tag{67}$$

$$\mathbb{P}(\text{proliferation to the right of cell } i \text{ in } [t,t+\mathrm{d}t)) = \begin{cases}\mathrm{d}t\displaystyle\sum_{j=i+1}^{N}G\big(x_j-x_{j-1}\big) & j\neq N,\\ 0 & j=N,\end{cases} \tag{68}$$

$$\mathbb{P}(\text{proliferation of cell } i \text{ in } [t,t+\mathrm{d}t)) = \mathrm{d}t\,G(x_i-x_{i-1}), \tag{69}$$

$$\mathbb{P}(\text{proliferation to the left of cell } i \text{ in } [t,t+\mathrm{d}t)) = \begin{cases}\mathrm{d}t\displaystyle\sum_{j=1}^{i-1}G\big(x_j-x_{j-1}\big) & j\neq 1,\\ 0 & j=1,\end{cases} \tag{70}$$

and

$$\mathbb{P}(\text{more than one cell proliferation event in } [t,t+\mathrm{d}t)) = \mathcal{O}\big(\mathrm{d}t^2\big). \tag{71}$$

We now take expectations on both sides of Eqs. (65) and (66), denoting by $\langle x_i^N(t)\rangle$ the expected position of node i at time t when there are N nodes. We then make two simplifying assumptions: (i) that $\langle x_i^N(t)\rangle$ is a continuous function of time; and (ii) that $\langle F(x_i^N(t))\rangle = F(\langle x_i^N(t)\rangle)$ and $\langle G(x_i^N(t))\rangle = G(\langle x_i^N(t)\rangle)$. The former assumes that the cell size is small relative to the tissue, and allows us to rearrange and take the limit as $\mathrm{d}t\to 0$ and, together with the latter (the standard mean-field approximation), we have

$$\langle x_0^N(t)\rangle = 0, \tag{72}$$

$$\begin{aligned}\eta\frac{\mathrm{d}}{\mathrm{d}t}\langle x_i^N(t)\rangle &= F\big(\langle x_i^N(t)\rangle-\langle x_{i-1}^N(t)\rangle\big)-F\big(\langle x_{i+1}^N(t)\rangle-\langle x_i^N(t)\rangle\big)\\ &\quad-\eta\langle x_i^{N-1}(t)\rangle\sum_{j=1}^{i}G\big(\langle x_j^{N-1}(t)\rangle-\langle x_{j-1}^{N-1}(t)\rangle\big)\\ &\quad+\frac{\eta}{2}\big(\langle x_i^{N-1}(t)\rangle+\langle x_{i-1}^{N-1}(t)\rangle\big)G\big(\langle x_i^{N-1}(t)\rangle-\langle x_{i-1}^{N-1}(t)\rangle\big)\\ &\quad+\eta\langle x_{i-1}^{N-1}(t)\rangle\sum_{j=1}^{i-1}G\big(\langle x_j^{N-1}(t)\rangle-\langle x_{j-1}^{N-1}(t)\rangle\big),\\ &\qquad i=1,\ldots,N-1,\end{aligned} \tag{73}$$

$$\begin{aligned}\eta\frac{\mathrm{d}}{\mathrm{d}t}\langle x_N^N(t)\rangle &= F\big(\langle x_N^N(t)\rangle-\langle x_{N-1}^N(t)\rangle\big)\\ &\quad-\eta\langle x_N^{N-1}(t)\rangle\sum_{j=1}^{N}G\big(\langle x_j^{N-1}(t)\rangle-\langle x_{j-1}^{N-1}(t)\rangle\big)\\ &\quad+\frac{\eta}{2}\big(\langle x_N^{N-1}(t)\rangle+\langle x_{N-1}^{N-1}(t)\rangle\big)G\big(\langle x_N^{N-1}(t)\rangle-\langle x_{N-1}^{N-1}(t)\rangle\big)\\ &\quad+\eta\langle x_{N-1}^{N-1}(t)\rangle\sum_{j=1}^{N-1}G\big(\langle x_j^{N-1}(t)\rangle-\langle x_{j-1}^{N-1}(t)\rangle\big).\end{aligned} \tag{74}$$

5.3. Continuum approximation

To enable a continuum approximation to be formulated we make the further approximation $\langle x_i^N(t)\rangle = \langle x_i^{N-1}(t)\rangle$, and to simplify exposition going forward, we will drop use of the angle brackets. After algebraic simplification, we have

$$x_0(t) = 0, \tag{75}$$

$$\begin{aligned}\eta\frac{\mathrm{d}x_i}{\mathrm{d}t} &= F(x_i-x_{i-1})-F(x_{i+1}-x_i)\\ &\quad-\eta(x_i-x_{i-1})\left[\sum_{j=1}^{i-1}G\big(x_j-x_{j-1}\big)+\frac{1}{2}G(x_i-x_{i-1})\right],\\ &\qquad i=1,\ldots,N-1,\end{aligned} \tag{76}$$

$$\begin{aligned}\eta\frac{\mathrm{d}x_N}{\mathrm{d}t} &= F(x_N-x_{N-1})\\ &\quad-\eta(x_N-x_{N-1})\left[\sum_{j=1}^{N-1}G\big(x_j-x_{j-1}\big)+\frac{1}{2}G(x_N-x_{N-1})\right].\end{aligned} \tag{77}$$

To make progress in deriving an equivalent continuum, coarse-grained model, we proceed as before: we extend node position, $x_i(t)$, to a smooth function $x(i,\,t)$ for $i\in[0,\,N(t)]$, and non-dimensionalise using the scalings

$$\tilde{i}=\frac{i}{N_0},\qquad \tilde{x}=\frac{x}{aN_0},\qquad \tilde{N}=\frac{N}{N_0},\qquad \tilde{t}=\frac{tka^{n-1}}{\eta N_0^2},$$

where $N_0=N(0)$, the number of nodes at $t=0$. We also define the non-dimensional proliferation function such that

$$\tilde{G}(\cdot)=\frac{\eta N_0}{ka^{n-1}}G(a\,\cdot), \tag{78}$$

and the non-dimensional force function is as specified in Eq. (44).

We then work in the same manner as before, using Taylor expansion together with quadrature approximations of the form

$$\sum_{j=1}^{i-1}G\big(x_j-x_{j-1}\big)+\frac{1}{2}G(x_i-x_{i-1})\approx\int_{j=0}^{i}G\big(x_j-x_{j-1}\big)\mathrm{d}j, \tag{79}$$

to give, upon neglecting terms that are $\mathcal{O}(1/N_0^2)$,

$$\begin{aligned}\frac{\partial\tilde{x}}{\partial\tilde{t}}+\frac{\partial\tilde{x}}{\partial\tilde{i}}\int_0^{\tilde{i}}\tilde{G}\left(\frac{\partial\tilde{x}}{\partial\tilde{j}}\right)\mathrm{d}\tilde{j} &= -\tilde{F}'\left(\frac{\partial\tilde{x}}{\partial\tilde{i}}\right)\frac{\partial^2\tilde{x}}{\partial\tilde{i}^2}\\ &\quad+\frac{1}{2N_0}\frac{\partial^2\tilde{x}}{\partial\tilde{i}^2}\int_0^{\tilde{i}}\tilde{G}\left(\frac{\partial\tilde{x}}{\partial\tilde{j}}\right)\mathrm{d}\tilde{j},\quad \tilde{i}\in[0,\tilde{N}(\tilde{t})].\end{aligned} \tag{80}$$

The left-hand boundary condition remains as $\tilde{x}(0,\tilde{t})=0$ and, once again, we derive the right-hand boundary condition by Taylor expanding and neglecting terms that are $\mathcal{O}(1/N^2)$ to give, at $\tilde{i}=\tilde{N}(\tilde{t})$,

$$\frac{1}{N_0}\frac{\partial \tilde{x}}{\partial \tilde{t}} = \tilde{F}\left(\frac{\partial \tilde{x}}{\partial \tilde{i}}\right) - \frac{1}{2N_0}\tilde{F}'\left(\frac{\partial \tilde{x}}{\partial \tilde{i}}\right)\frac{\partial^2 \tilde{x}}{\partial \tilde{i}^2} - \frac{1}{N_0}\frac{\partial \tilde{x}}{\partial \tilde{i}}\int_0^{\tilde{N}} \tilde{G}\left(\frac{\partial \tilde{x}}{\partial \tilde{j}}\right)\mathrm{d}\tilde{j}. \tag{81}$$

Rewriting Eq. (80) in terms of the dimensional variables we have the following PDE for $x(i, t)$:

$$\eta\frac{\partial x}{\partial t} + \eta\frac{\partial x}{\partial i}\int_0^i G\left(\frac{\partial x}{\partial j}\right)\mathrm{d}j = -F'\left(\frac{\partial x}{\partial i}\right)\frac{\partial^2 x}{\partial i^2} + \frac{\eta}{2}\frac{\partial^2 x}{\partial i^2}\int_0^i G\left(\frac{\partial x}{\partial i}\right)\mathrm{d}j \quad i \in (0, N(t)). \tag{82}$$

The boundary conditions are

$$x(0,t) = 0 \quad \text{and} \quad \eta\frac{\partial x}{\partial t}\bigg|_{i=N(t)} = \left[F\left(\frac{\partial x}{\partial i}\right) - \frac{1}{2}\frac{\partial^2 x}{\partial i^2}F'\left(\frac{\partial x}{\partial i}\right) - \eta\frac{\partial x}{\partial i}\int_0^i G\left(\frac{\partial x}{\partial j}\right)\mathrm{d}j\right]\bigg|_{i=N(t)}. \tag{83}$$

As before, the initial conditions can be specified by extending the discrete initial conditions, $x_i(0) = x_i^0$ for $i = 1, \ldots, N(0)$, to a continuous function $x(i, 0)$ such that $x(i, 0) = x_i^0$ for $i = 1, \ldots, N(0)$.

5.4. Derivation of the corresponding cell density model

We now establish a PDE describing the evolution of cell density with position, x, and time, t, for a proliferative cell population with general force and proliferation laws. Changing variables from (i, t) to (x, τ), as before, with a simple substitution of terms from Eqs. (19) and (20) into Eq. (82) we obtain the PDE

$$\eta\frac{\partial x}{\partial \tau} + \frac{\eta}{q}\int_0^x q\,G\left(\frac{1}{q}\right)\mathrm{d}y = \frac{1}{q^3}F'\left(\frac{1}{q}\right)\frac{\partial q}{\partial x} - \frac{\eta}{2q^3}\frac{\partial q}{\partial x}\int_0^x q\,G\left(\frac{1}{q}\right)\mathrm{d}y, \quad x \in [0, L(\tau)], \tag{84}$$

which represents how the domain evolves along the characteristics. Note that, due to proliferation, this is no longer equivalent to following constant cell index, i.

After further rearrangement, as before, we have

$$\frac{\partial q}{\partial \tau} = \frac{\partial}{\partial x}\left(\left[D(q) + E(q)\right]\frac{\partial q}{\partial x}\right) + q\,G\left(\frac{1}{q}\right), \qquad x \in (0, L(\tau)), \tag{85}$$

where

$$D(q) = -\frac{1}{\eta q^2}F'\left(\frac{1}{q}\right) \qquad \text{and} \qquad E(q) = \frac{1}{2q^2}\int_0^x q\,G\left(\frac{1}{q}\right)\mathrm{d}y. \tag{86}$$

Under the same change of variables, the boundary conditions become

$$\frac{\partial q}{\partial x}\bigg|_{x=0} = 0 \quad \text{and} \quad \left[\frac{1}{\eta}F\left(\frac{1}{q}\right) + \left(\frac{D(q)}{2q} + \frac{E(q)}{q}\right)\frac{\partial q}{\partial x}\right]\bigg|_{x=L(\tau)} = 0, \tag{87}$$

and the initial conditions, computed as in Section 3.1, are

$$q(x, 0) = q_0(x), \qquad x \in (0, L(0)). \tag{88}$$

Using Eq. (86), characteristic Eq. (84) can be re-written as

$$\frac{\mathrm{D}x}{\mathrm{D}\tau} = \frac{\partial x}{\partial \tau} + \frac{1}{q}\int_0^x q\,G\left(\frac{1}{q}\right)\mathrm{d}y = -\frac{1}{q}\left[D(q) + E(q)\right]\frac{\partial q}{\partial x}, \quad x \in [0, L(\tau)], \tag{89}$$

That the left-hand side of Eq. (89) constitutes a material derivative can be seen by following a small "tissue element" as the cell population grows and divides. We have $x = x(i(t), t)$ with

$$\frac{\mathrm{D}x}{\mathrm{D}\tau} = \frac{\partial x}{\partial \tau} + \frac{\partial x}{\partial i}\frac{\partial i}{\partial \tau} = \frac{\partial x}{\partial \tau} + \frac{1}{q}\int_0^x q\,G\left(\frac{1}{q}\right)\mathrm{d}y, \tag{90}$$

where we have used the fact that the rate of change of cell index is equal to the rate of cell proliferation in the region to the left of the cell *i.e.*

$$\frac{\partial i}{\partial \tau} = \int_0^x q\,G\left(\frac{1}{q}\right)\mathrm{d}y. \tag{91}$$

Finally, using Eq. (89) we can specify the rate of growth of the domain over time as

$$\frac{\mathrm{d}L(\tau)}{\mathrm{d}\tau} = \left(-\frac{1}{q}\left[D(q) + E(q)\right]\frac{\partial q}{\partial x}\right)\bigg|_{L(\tau)}. \tag{92}$$

5.5. Evolution of cell number

Note that, since cell proliferation is now present in the model, the cell number changes over time and the system does not conserve mass. The cell number at time τ is specified by Eq. (18) as

$$N(\tau) = \int_0^{L(\tau)} q(x, \tau)\,\mathrm{d}x. \tag{93}$$

Differentiating with respect to τ and using the left-hand boundary condition (97) gives

$$\begin{aligned}\frac{\mathrm{d}N}{\mathrm{d}\tau} &= \frac{\mathrm{d}L}{\mathrm{d}\tau}q(L(\tau), \tau) + \int_0^{L(\tau)}\frac{\partial q}{\partial \tau}(x, \tau)\,\mathrm{d}x,\\ &= \frac{\mathrm{d}L}{\mathrm{d}\tau}q(L(\tau), \tau)\\ &\quad + \int_0^{L(\tau)}\left\{\frac{\partial}{\partial x}\left(\left[D(q) + E(q)\right]\frac{\partial q}{\partial x}\right) + q\,G\left(\frac{1}{q}\right)\right\}\mathrm{d}x,\\ &= \left[\frac{\mathrm{d}L}{\mathrm{d}\tau}q + \left[D(q) + E(q)\right]\frac{\partial q}{\partial x}\right]\bigg|_{x=L(\tau)} + \int_0^{L(\tau)} q\,G\left(\frac{1}{q}\right)\mathrm{d}x,\end{aligned} \tag{94}$$

Substituting Eq. (92) into Eq. (94) gives the rate of change of cell number over time as

$$\frac{\mathrm{d}N}{\mathrm{d}\tau} = \int_0^{L(\tau)} q\,G\left(\frac{1}{q}\right)\mathrm{d}y. \tag{95}$$

This equation states simply and intuitively that the rate of change of cell number is simply equal to the sum of the proliferation rates of each cell.

5.6. Numerical solution

In summary, the coarse-grained model consists of a PDE for the evolution of cell density

$$\frac{\partial q}{\partial \tau} = \frac{\partial}{\partial x}\left(\left[D(q) + E(q)\right]\frac{\partial q}{\partial x}\right) + q\,G\left(\frac{1}{q}\right), \qquad x \in (0, L(\tau)), \tag{96}$$

together with boundary conditions

$$\frac{\partial q}{\partial x}\bigg|_{x=0} = 0 \quad \text{and} \quad \left[\frac{1}{\eta}F\left(\frac{1}{q}\right) + \left(\frac{D(q)}{2q} + \frac{E(q)}{q}\right)\frac{\partial q}{\partial x}\right]\bigg|_{x=L(\tau)} = 0, \tag{97}$$

and initial condition

$$q(x, 0) = q_0(x), \qquad x \in (0, L(0)). \tag{98}$$

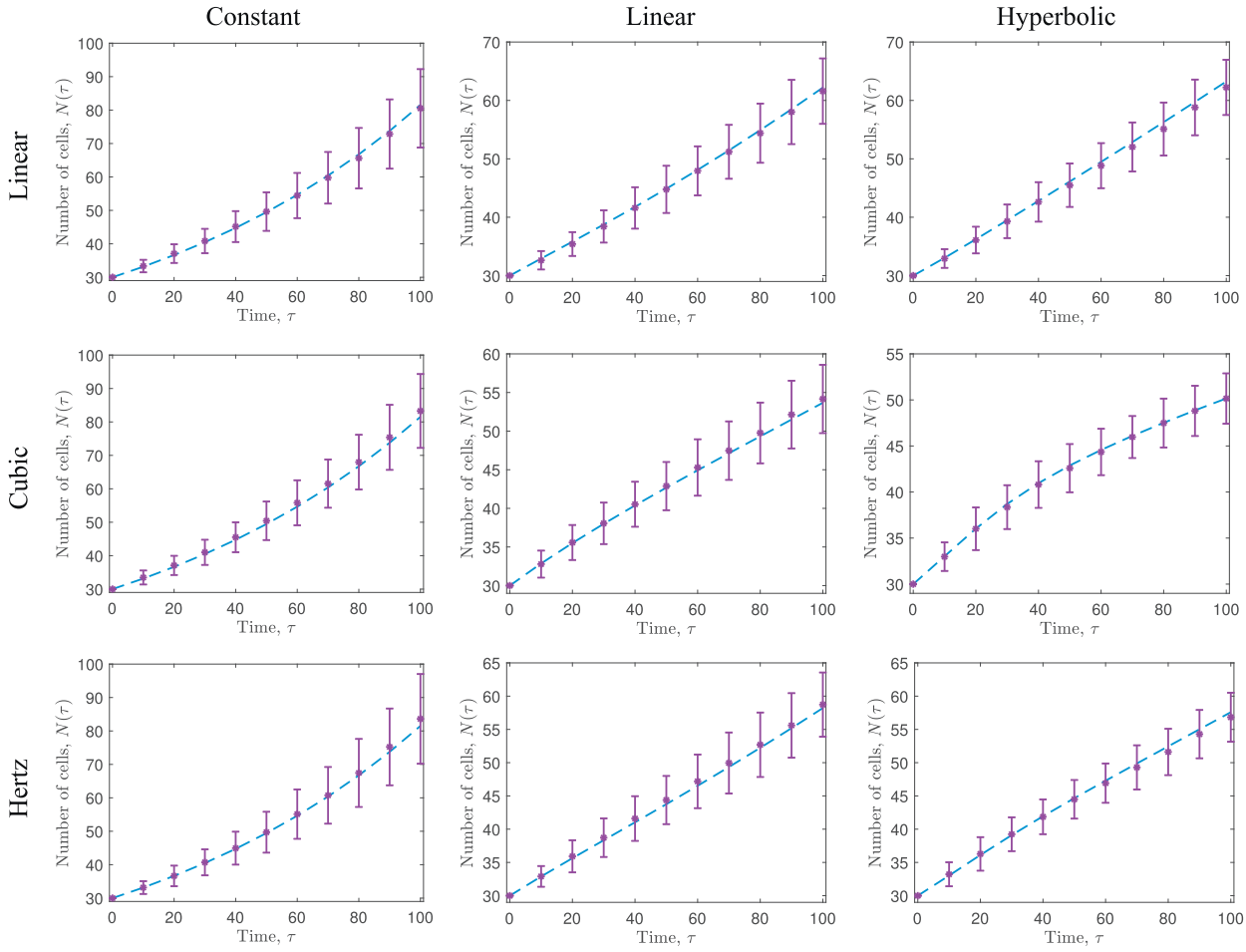

Fig. 7. Comparison of the number of cells, $N(\tau)$, predicted by the cell-based model described in Section 5.1 (purple asterisks, and accompanying error bars (mean ± one standard deviation)), and the coarse-grained model, Eqs. (96)–(100) (blue dashed line), for varying force laws and proliferation functions. Each row represents a different force law, whereas each column represents a different proliferation function. Each force law is defined and visualised in Fig. 3, and each proliferation function is defined and visualised in Fig. 6. In each case, we display averaged results from 100 realisations of the stochastic model, $N = 30$ cells are initialised uniformly in $x \in (0, 30)$ and $a = 1$, $\alpha = 15$, and $\beta = 0.001$. (For interpretation of the references to colour in this figure legend, the reader is referred to the web version of this article.)

The characteristic equation is

$$\frac{\mathrm{D}x}{\mathrm{D}\tau} = \frac{\partial x}{\partial \tau} + \frac{1}{q}\int_0^x q\, G\left(\frac{1}{q}\right)\mathrm{d}y = -\frac{1}{q}\left[D(q)+E(q)\right]\frac{\partial q}{\partial x}, \quad x \in [0, L(\tau)], \tag{99}$$

and we have

$$\frac{\mathrm{d}L(\tau)}{\mathrm{d}\tau} = \left(-\frac{1}{q}\left[D(q)+E(q)\right]\frac{\partial q}{\partial x}\right)\bigg|_{L(\tau)}. \tag{100}$$

As in Sections 3.2.1 and 4.2.1, in order to solve the coarse-grained model numerically, we employ a Lagrangian transformation to map the free boundary problem to a fixed domain: we let $\tau = T$ and

$$x = \Gamma(X, T) \text{ with } X = \Gamma(X, 0), \;\; 0 = \Gamma(0, T), \;\; L(T) = \Gamma(L(0), T), \tag{101}$$

to give

$$\frac{\partial \Gamma}{\partial T} = -\frac{D(q)+E(q)}{q\Gamma_X}\frac{\partial q}{\partial X}, \quad X \in (0, L(0)), \tag{102}$$

$$\frac{\partial q}{\partial T} - \frac{1}{\Gamma_X}\frac{\partial \Gamma}{\partial T}\frac{\partial q}{\partial X} = \frac{1}{\Gamma_X}\frac{\partial}{\partial X}\left(\frac{D(q)+E(q)}{\Gamma_X}\frac{\partial q}{\partial X}\right) + q\, G\left(\frac{1}{q}\right), \quad X \in (0, L(0)). \tag{103}$$

The initial and boundary conditions for $\Gamma(X, T)$ are specified in Eq. (101), and for $q(X, T)$ we have

$$\frac{\partial q}{\partial X}\bigg|_{X=0} = 0 \qquad \text{and} \qquad \left[\frac{1}{\eta}F\left(\frac{1}{q}\right) + \frac{1}{q\Gamma_X}\left(\frac{D(q)}{2} + E(q)\right)\frac{\partial q}{\partial X}\right]\bigg|_{X=L(0)} = 0, \tag{104}$$

together with

$$q(X, 0) = q_0(X) \qquad X \in (0, L(0)). \tag{105}$$

We solve the model numerically using an implicit finite difference method with Picard iteration. Full details are given in Appendix B.

5.7. Results

To demonstrate the validity of the coarse-grained model, we compare the solution of the PDE system, Eqs. (96)–(100), with 100 averaged realisations of the discrete, stochastic model. Across all force laws and proliferation functions tested, the coarse-grained PDE model is very accurate in its prediction of both evolution of the mean cell number, $N(\tau)$, and the mean position of the free boundary at $x = L(\tau)$ (see Figs. 7 and 8, respectively).[4] The differ-

[4] For example, the agreement of the models for varying α/β (doubled and halved) is also excellent (results not shown).

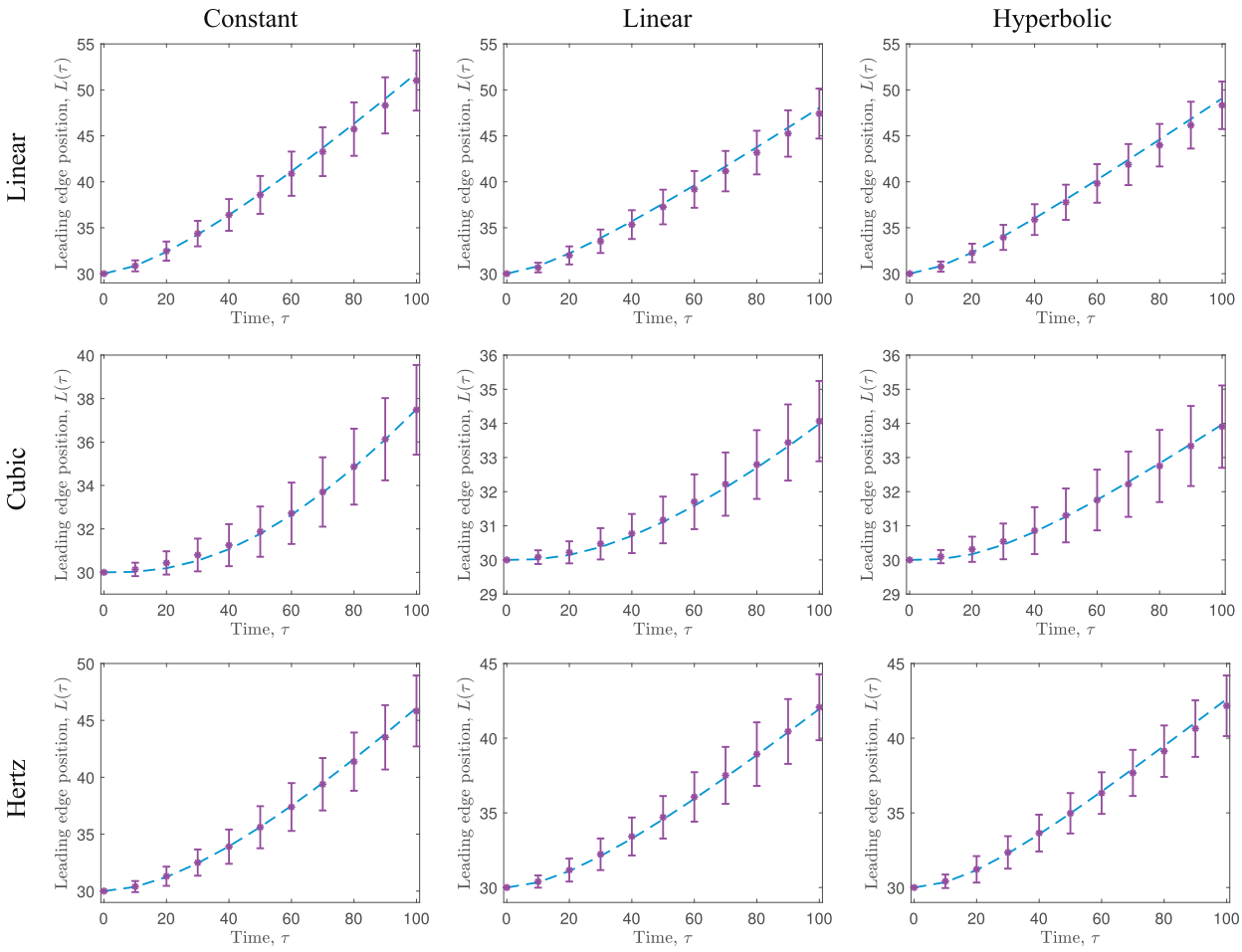

Fig. 8. Comparison of the leading edge position, $L(\tau)$, predicted by the cell-based model described in Section 5.1 (purple asterisks, and accompanying error bars (mean $\pm$ one standard deviation)), and the coarse-grained model, Eqs. (96)–(100) (blue dashed line), for varying force laws and proliferation functions. Each row represents a different force law, whereas each column represents a different proliferation function. Each force law is defined and visualised in Fig. 3, and each proliferation function is defined and visualised in Fig. 6. In each case, we display averaged results from 100 realisations of the stochastic model, $N = 30$ cells are initialised uniformly in $x \in (0,\ 30)$ and $a = 1$, $\alpha = 15$, and $\beta = 0.001$. (For interpretation of the references to colour in this figure legend, the reader is referred to the web version of this article.)

ent force laws and proliferation functions result in quite different behaviours, in particular how quickly the leading edge expands or how rapidly the number of cells increases.

6. Discussion and outlook

In this work we study a one-dimensional cell-based model of an epithelial sheet of cells where individual cells move deterministically and proliferate stochastically. This cell-based mechanical model gives rise to a moving boundary problem on the domain $0 < x < L(\tau)$, where τ is time. We construct a continuum-limit description of the cell-based model, leading to a novel moving boundary PDE description governing the density of the cells within the evolving domain, $0 < x < L(\tau)$, as well as a moving boundary condition governing the evolution of $L(\tau)$. Our results show that care must be taken to arrive at a moving boundary condition that conserves mass appropriately.

There are many ways that our modelling approach can be extended, both from a theoretical point of view and a biological point of view. In all cases considered, we always study problems leading to an expanding population of cells where $L(\tau)$ is an increasing function of time. While these sets of problems are biologically relevant since they correspond to growing tissues, an interesting extension of our work would be to consider incorporating cell death and cell extrusion so that the model can be used to study both tissue growth and tissue shrinkage (Yates, 2014). Other avenues for interesting extensions would be to consider the incorporation of internal boundaries within a mixed heterogeneous population so that the model could be used to study the interactions between an invasive population, such as a population of tumour cells, that invades into a surrounding population of non-invasive cells (Haridas et al., 2017). Furthermore, an obvious extension of the current work would be to two or three dimensions (Smith et al., 2012; Zmurchok et al., 2018). In terms of biological applications, mechanical models describing cell migration and cell proliferation are important in wound healing (Evans et al., 2013), development (Kular et al., 2015), and cancer progression (Samuel et al., 2011) and detection (Huo et al., 2014). In all of these various applications we expect that experimental and clinical data will encompass both individual cell-based information as well as population-level, tissue-scale information. Therefore, the general framework of developing and applying cell-based models to study a particular phenomena while simultaneously working with a coarse-grained approximation to provide population-level information will be important to ensure that we get the most out of taking a combined modelling and experimental approach to studying particular biological phenomena.

Acknowledgements

REB is a Royal Society Wolfson Research Merit Award holder, would like to thank the Leverhulme Trust for a Research Fellowship, and also acknowledges the BBSRC for funding via grant no. BB/R000816/1. AP would like to thank the UK's Engineering and Physical Sciences Research Council (EPSRC, EP/G03706X/1) for funding through a studentship at the Systems Biology programme of The University of Oxford's Doctoral Training Centre. MJS appreciates support from the Australian Research Council (DP170100474). The authors would also like to thank two anonymous referees for their constructive comments.

Appendix A. Boundary condition derivation

We derive the transformed boundary condition, starting from Eq. (21)

$$\begin{aligned}
\frac{\partial x}{\partial t} &= \alpha\left(a - \frac{\partial x}{\partial i} + \frac{1}{2}\frac{\partial^2 x}{\partial i^2}\right),\\
-\frac{\alpha}{q^3}\frac{\partial q}{\partial x} &= \alpha\left(a - \frac{1}{q} + \frac{1}{2}\frac{\partial}{\partial i}\left(\frac{1}{q}\right)\right),\\
-\frac{\alpha}{q^3}\frac{\partial q}{\partial x} &= \alpha\left(a - \frac{1}{q} + \frac{1}{2}\frac{\partial x}{\partial i}\frac{\partial}{\partial x}\left(\frac{1}{q}\right)\right),\\
-\frac{\alpha}{q^3}\frac{\partial q}{\partial x} &= \alpha\left(a - \frac{1}{q} + \frac{1}{2q}\left(-\frac{1}{q^2}\frac{\partial q}{\partial x}\right)\right),\\
0 &= aq - 1 + \frac{1}{2}\frac{1}{q^2}\frac{\partial q}{\partial x}.
\end{aligned}$$

Appendix B. Numerical solution of the full system

We solve Eqs. (101)–(105) numerically using a finite difference scheme with Picard iteration. Algorithm 1 provides the scheme

Algorithm 1 Picard iteration for the PDE system, Eqs. (101)–(105), derived in Section 5.6.

```
τ = 0, k = 1
while τ < T do
    for j = 1 to j = J do
        if k = 1 then
            q_j^k = q_j^(prev), Γ_j^k = Γ_j^(prev)
        end if
        Solve for Γ_j^{k+1} using q_{j-1}^k, q_j^k, q_{j+1}^k and Γ_{j-1}^k, Γ_j^k, Γ_{j+1}^k
        Solve for q_j^{k+1} using q_{j-1}^k, q_j^k, q_{j+1}^k and Γ_j^{k+1}, Γ_{j-1}^{k+1}, Γ_{j+1}^{k+1}
    end for
    if d(q^k, q^{k+1}) < ϵ then
        q^(prev) = q^{k+1}, Γ^(prev) = Γ^{k+1}
        k = 1
        τ = τ + dτ
    else
        k = k + 1
    end if
end while
```

used for Picard iteration. The tolerance for the Picard iteration step is $\epsilon = 10^{-4}$, where the distance between solutions, $d(q^k, q^{k+1})$, is computed using the sum of squared differences over all space points, and the space step and time step are $dX = 0.01$ and $d\tau = 0.001$, respectively.

Within the Picard algorithm, Eq. (102) is discretised as

$$\Gamma_j^{k+1} = \Gamma_j^{(prev)} - \delta\tau\frac{D\left(q_j^k\right) + E\left(q_j^k\right)}{q_j^k}\frac{q_{j+1}^k - q_{j-1}^k}{\Gamma_{j+1}^k - \Gamma_{j-1}^k}, \tag{B.1}$$

and Eq. (103) as

$$\begin{aligned}
q_j^{k+1} = q_j^{(prev)} + \delta\tau\Bigg\{ & q_j^k G\left(q_j^k\right) + \frac{\Gamma_j^{k+1} - \Gamma_j^{(prev)}}{\delta t}\frac{q_{j+1}^{k+1} - q_{j-1}^{k+1}}{\left(\Gamma_{j+1}^{k+1} - \Gamma_{j-1}^{k+1}\right)^2}\\
& + \frac{2\delta X}{\Gamma_{j+1}^{k+1} - \Gamma_{j-1}^{k+1}}\frac{1}{\delta X}\left[\frac{D\left(q_{j+1}^k\right) + D\left(q_j^k\right)}{2}\right.\\
& \left. + \frac{E\left(q_{j+1}^k\right) + E\left(q_j^k\right)}{2}\right]\frac{q_{j+1}^{k+1} - q_j^{k+1}}{\Gamma_{j+1}^{k+1} - \Gamma_j^{k+1}}\\
& - \frac{2\delta X}{\Gamma_{j+1}^{k+1} - \Gamma_{j-1}^{k+1}}\frac{1}{\delta X}\left[\frac{D\left(q_j^k\right) + D\left(q_{j-1}^k\right)}{2}\right.\\
& \left. + \frac{E\left(q_j^k\right) + E\left(q_{j-1}^k\right)}{2}\right]\frac{q_j^{k+1} - q_{j-1}^{k+1}}{\Gamma_j^{k+1} - \Gamma_{j-1}^{k+1}}\Bigg\},
\end{aligned} \tag{B.2}$$

where the subscript, j, indexes the space step, the superscript, k, the Picard iteration step. Eq. (B.2) can be rearranged to give

$$\begin{aligned}
q_j^{k+1} = {} & q_j^k + \delta\tau\, q_j^k G(q_j^k)\\
& + \delta\tau\left[-\frac{\Gamma_j^{k+1} - \Gamma_j^{(prev)}}{\delta t\left(\Gamma_{j+1}^{k+1} - \Gamma_{j-1}^{k+1}\right)^2}\right.\\
& \left. + \frac{D(q_j^k) + D(q_{j-1}^k) + E(q_j^k) + E(q_{j-1}^k)}{\left(\Gamma_j^{k+1} - \Gamma_{j-1}^{k+1}\right)\left(\Gamma_{j+1}^{k+1} - \Gamma_{j-1}^{k+1}\right)}\right]q_{j-1}^{k+1}\\
& + \delta\tau\left[-\frac{D(q_{j+1}^k) + D(q_j^k) + E(q_{j+1}^k) + E(q_j^k)}{\left(\Gamma_{j+1}^{k+1} - \Gamma_j^{k+1}\right)\left(\Gamma_{j+1}^{k+1} - \Gamma_{j-1}^{k+1}\right)}\right.\\
& \left. - \frac{D(q_j^k) + D(q_{j-1}^k) + E(q_j^k) + E(q_{j-1}^k)}{\left(\Gamma_j^{k+1} - \Gamma_{j-1}^{k+1}\right)\left(\Gamma_{j+1}^{k+1} - \Gamma_{j-1}^{k+1}\right)}\right]q_j^{k+1}\\
& + \delta\tau\left[\frac{\Gamma_j^{k+1} - \Gamma_j^{(prev)}}{\delta t(\Gamma_{j+1}^{k+1} - \Gamma_{j-1}^{k+1})^2}\right.\\
& \left. + \frac{D(q_{j+1}^k) + D(q_j^k) + E(q_{j+1}^k) + E(q_j^k)}{\left(\Gamma_{j+1}^{k+1} - \Gamma_j^{k+1}\right)\left(\Gamma_{j+1}^{k+1} - \Gamma_{j-1}^{k+1}\right)}\right]q_{j+1}^{k+1},
\end{aligned} \tag{B.3}$$

and then solved using the tridiagonal matrix algorithm.

Supplementary material

Supplementary material associated with this article can be found, in the online version, at doi:10.1016/j.jtbi.2018.12.025.

References

Anderson, A.R.A., Chaplain, M.A.J., 1998. Continuous and discrete mathematical models of tumor-induced angiogenesis. Bull. Math. Biol. 60, 857–859.

Browning, A.P., McCue, S.W., Binny, R.N., Plank, M.J., Shah, E.T., Simpson, M.J., 2018. Inferring parameters for a lattice-free model of cell migration and proliferation using experimental data. J. Theor. Biol. 437, 251–260.

Cai, A.Q., Landman, K.A., Hughes, B.D., 2007. Multi-scale modeling of a wound-healing cell migration assay. J. Theor. Biol. 245, 576–594.

Evans, N.D., Oreffo, R.O.C., Healy, E., Thurner, P.J., Man, Y.H., 2013. Epithelial mechanobiology, skin wound healing, and the stem cell niche. J. Mech. Behav. Biomed.Mater. 28, 397–409.

Fozard, J.A., Byrne, H.M., Jensen, O.E., King, J.R., 2009. Continuum approximations of individual-based models for epithelial monolayers. Math. Med. Biol. 27, 39–74.

Gelman, A., Carlin, J., Stern, H., Dunson, D., Vehtari, A., Rubin, D., 2013. Bayesian data analysis, Third Edition Chapman and Hall/CRC.

Haridas, P., McGovern, J.A., McElwain, D.L.S., Simpson, M.J., 2017. Quantitative comparison of the spreading and invasion of radial growth phase and metastatic melanoma cells in a three-dimensional human skin equivalent model. Peer J. 5, e3754.

Huo, C.W., Chew, G.L., Britt, K.L., Ingman, W.V., Henderson, M.A., Hopper, J.L., Thompson, E.W., 2014. Mammographic density a review on the current understanding of its association with breast cancer. Breast Cancer Res. Treat. 144, 479–502.

Jin, W., McCue, S.W., Simpson, M.J., 2018. Extended logistic growth model for heterogeneous populations. J. Theor. Biol. 445, 51–61.

Jin, W., Shah, E.T., Penington, C.J., McCue, S.W., Chopin, L.K., Simpson, M.J., 2016. Reproducibility of scratch assays is affected by the initial degree of confluence: experiments, modelling and model selection. J. Theor. Biol. 390, 136–145.

Kular, J., Scheer, K.G., Pyne, N.T., Allam, A.H., Pollard, A.N., Magenau, A., Wright, R.L., Kolesnikoff, N., Moretti, P.A., Wullkopf, L., Stomski, F.C., Cowin, A.J., Woodcock, J.M., Grimbaldeston, M.A., Pitson, S.M., Timpson, P., Ramshaw, H.S., Lopez, A.F., Samuel, M.S., 2015. A negative regulatory mechanism involving 14-3-3ζ limits signaling downstream of rock to regulate tissue stiffness in epidermal homeostasis. In: Developmental Cell, Vol. 35, pp. 759–774.

Maini, P.K., McElwain, D.L.S., Leavesley, D., 2004. Travelling waves in a wound healing assay. Appl. Math. Lett. 17, 575–580.

Maini, P.K., McElwain, D.L.S., Leavesley, D.I., 2004. Traveling wave model to interpret a wound-healing cell migration assay for human peritoneal mesothelial cells. Tissue Eng. 10, 475–482.

Murray, P.J., Edwards, C.M., Tindall, M.J., Maini, P.K., 2009. From a discrete to a continuum model of cell dynamics in one dimension. Phys. Rev. E 80, 031912.

Murray, P.J., Edwards, C.M., Tindall, M.J., Maini, P.K., 2012. Classifying general nonlinear force laws in cell-based models via the continuum limit. Phys. Rev. E 85, 021921.

Murray, P.J., Walter, A., Fletcher, A.G., Edwards, C.M., Tindall, M.J., Maini, P.K., 2011. Comparing a discrete and continuum model of the intestinal crypt. Phys. Biol. 8, 026011.

O'Dea, R., King, J.R., 2012. Continuum limits of pattern formation in hexagonal cell monolayers. J Math Biol 64, 579–610.

Osborne, J.M., Fletcher, A.G., Pitt-Francis, J.M., Maini, P.K., Gavaghan, D.J., 2017. Comparing individual-based approaches to modelling the self-organization of multicellular tissues. PLoS Comput. Biol. 13, e1005387.

Parker, A., Simpson, M.J., Baker, R.E., 2018. The impact of experimental design choices on parameter inference for models of growing cell colonies. R. Soc. Open Sci. 5, 180384.

Pathmanathan, P., Cooper, J., Fletcher, A., Mirams, G., Murray, P., Osborne, J., Pitt-Francis, J., Walter, A., Chapman, S.J., 2009. A computational study of discrete mechanical tissue models. Phys. Biol. 6, 036001.

Samuel, M.S., Lopez, J.I., McGhee, E.J., Croft, D.R., Strachan, D., Timpson, P., Munro, J., Schroder, E., Zhou, J., Brunton, V.G., Barker, N., Clevers, H., Sansom, O.J., Anderson, K.I., Weaver, V.M., Olson, M.F., 2011. Actomyosin-mediated cellular tension drives increased tissue stiffness and beta-catenin activation to induce epidermal hyperplasia and tumor growth. Cancer Cell 19, 776–791.

Simpson, M.J., Treloar, K.K., Binder, B.J., Haridas, P., Manton, K.J., Leavesley, D.I., McElwain, D.L.S., Baker, R.E., 2013. Quantifying the roles of cell motility and cell proliferation in a circular barrier assay. J. R. Soc. Interface 10, 20130007.

Smith, A.M., Baker, R.E., Kay, D., Maini, P.K., 2012. Incorporating chemical signalling factors into cell-based models of growing epithelial tissues. J. Math. Biol. 65, 441–463.

Treloar, K.K., Simpson, M.J., McElwain, D.L.S., Baker, R.E., 2014. Are *in vitro* estimates of cell diffusivity and cell proliferation rate sensitive to assay geometry? J. Theor. Biol. 356, 71–84.

Turner, S., Sherratt, J.A., Painter, K.J., Savill, N.J., 2004. From a discrete to a continuous model of biological cell movement. Phys. Rev. E 69, 021910.

Yates, C.A., 2014. Discrete and continuous models for tissue growth and shrinkage. J. Theor. Biol. 350, 37–48.

Zmurchok, C., Bhaskar, D., Edelstein-Keshet, L., 2018. Coupling mechanical tension and GTPase signaling to generate cell and tissue dynamics. Phys. Biol. 15, 046004.